Modeling Human Head Tissues Using Fourth-Order Debye Model in Convolution-Based Three-Dimensional Finite-Difference Time-Domain

S. Mustafa, A. Abbosh , *Senior member IEEE,* P. Nguyen

***Abstract*—A fourth order Debye model is derived using genetic algorithms to represent the dispersive properties of the 17 tissues that form the human head. The derived model gives accurate estimation of the electrical properties of those tissues across the frequency band from 0.1 GHz to 3 GHz that can be used in microwave systems for head imaging. A convolution-based three-dimensional finite-difference time-domain (3D-FDTD) formulation is implemented for modeling the electromagnetic wave propagation in the dispersive head tissues whose frequency dependent properties are represented by the derived fourth-order Debye model. The presented results show that the proposed 3D-FDTD and fourth-order Debye model can accurately show the electromagnetic interaction between a wide band radiation and head tissues with low computational overhead and more accurate results compared with using multi-pole Cole-Cole model.**

Keywords— Debye model; head modeling; finite-difference time-domain; microwave imaging; microwave modeling; Cole-Cole model.

I. INTRODUCTION

Microwave imaging systems have increasingly been investigated for medical applications [1]-[11]. One of those emerging applications is the head imaging for stroke detection [7]-[11]. In such an application, the analysis of the microwave's penetration in the head tissues is increasingly of interest using either integral-based method of moments (MOM) [10] or the finite-difference time-domain (FDTD) method [11].

Since microwave imaging systems usually use wide frequency bands in their operation, the dispersive properties of the tissues are of a major concern to get meaningful imaging results. In MOM, tissues' properties can be assigned at each unique frequency simulation. The FDTD method, however, requires a more elaborate approach in order to maintain its advantageous feature, i.e. simultaneous simulation of a large bandwidth. An accurate time-domain modeling of the tissues' properties is incorporated by enforcing a model of the change in the complex dielectric permittivity in the governing field equations.

Manuscript received March 12, 2013, revised November 18, 2013, accepted December 17, 2013. This work was supported by the Faculty for Future, Endeavour Research Fellowships and the Australian Research Council Discovery Grant DP120101214.

The authors are with the School of Information Technology and Electrical Engineering, University of Queensland, St. Lucia, Brisbane QLD 4072, Australia. S. Mustafa is also affiliated with College of Engineering, Salahaddin University, Erbil, Iraq (e-mail: samah.mustafa@uq.edu.au; a.abbosh@uq.edu.au).

The finite-difference time-domain (FDTD) method has been widely used for numerical calculations of electromagnetic wave propagation in biological tissues [12]-[14]. Since the electrical properties of biological tissues are frequency dependent, the accuracy of FDTD is dependent in part on the accuracy of the used dispersion model. In [13], the complex permittivity of many types of biological tissues is modeled using a Cole-Cole formulation. However, the analysis using FDTD with the Cole–Cole model is not straightforward and produces computational complexity. Various modalities have been developed to implement Cole-Cole dispersion relation in FDTD codes [15]-[19]. However, those methods result in a lower accuracy, or a time consuming procedure.

Besides the computational complexity when using the Cole-Cole model in FDTD, the available Cole-Cole model for brain tissues doesn't perfectly fit the real experimental data over the entire spectrum. Thus, other options that require least computational overhead and can incorporate the dispersion into the FDTD method, such as Debye model, have gained significant interests [20], [21]. Recently, Ireland and Abbosh [21] have used a mean square error function to fit the experimental data of eight head tissues (grey matter, white matter, fat, CSF, dura, skin, blood and skull) to a second order Debye model.

It is well known that the accuracy of the Debye model in representing the dispersive properties of biological tissues over a wide frequency band depends on the number of utilized terms [20]. Thus, a higher order model that represents not just the main tissues of the head, but all the seventeen tissue types across the band being utilized for head imaging is required. That model needs to be still easily implemented in the FDTD method.

In this work, we develop a highly accurate fourth-order Debye model that perfectly fits the real experiment data [22] of the whole seventeen tissue types in the head across the band 0.1-3 GHz using genetic algorithm for the optimization purpose. The frequency range 0.1-3 GHz is chosen as it is widely used in head imaging for a reasonable compromise between penetration and resolution. We then present three-dimensional FDTD implementation based on the general convolution approach using the derived fourth-order Debye model. Verification to the accuracy of the developed fourth order Debye model and the 3D-FDTD implementation is quantified in this paper.

II. Optimization Process to Formulate the Electric Properties of Head Tissues

In this work, a fourth-order Debye model is derived for each of the seventeen tissue types in the human head. To obtain the best estimate of the Debye parameters compared with measured data from [22], a genetic algorithm is used in the optimization.

A. Fourth-Order Debye Model for Head Tissues

Frequency dependent materials can be accurately represented by the P[th]-order Cole-Cole formulation [13] given by

$$\mathcal{E}_r'(\omega) = \mathcal{E}_\infty + \sum_{i=1}^{P} \frac{\Delta\mathcal{E}_i}{(1+j\omega\tau_i)^{1-\alpha_i}} + \frac{\sigma_s}{j\omega\mathcal{E}_0} \qquad (1)$$

$\mathcal{E}_0$ denotes the permittivity of free space and $\mathcal{E}_\infty$ the permittivity at infinite frequency. The dispersion is given by $\Delta\mathcal{E}_i = \mathcal{E}_{Si} - \mathcal{E}_\infty$, where $\mathcal{E}_{Si}$ is the static permittivity at which the angular frequency ω multiple the relaxation time τ_i, i.e. $(\omega\tau_i) << 1$. The exponent α_i stretches the relaxation over a wide frequency range. σ_s is the static conductivity.

The complex relative permittivity $\mathcal{E}_r'(\omega)$ as a function of angular frequency is composed of frequency dependent permittivity $\mathcal{E}(\omega)$ and conductivity $\sigma(\omega)$. It is expressed in terms of Debye model of five terms in addition to a conductivity term in which σ_s is the static value.

$$\mathcal{E}_r'(\omega) = \mathcal{E}_\infty + \sum_{i=1}^{4} \frac{\Delta\mathcal{E}_i}{1+j\omega\tau_i} + \frac{\sigma_s}{j\omega\mathcal{E}_0} \qquad (2)$$

In this work, the genetic algorithm is used to minimize an error function € that is defined here as an objective function to derive the Debye parameters with excellent fit to the experimental data at each used individual radian frequency ω_k. The utilized error function is defined by [20]

$$€ = \frac{\sum_{k=1}^{N}\left[\frac{\mathcal{E}(\omega_k)-\mathcal{E}_d(\omega_k)}{median[\mathcal{E}_d(\omega)]}\right]^2 + \sum_{k=1}^{N}\left[\frac{\sigma(\omega_k)-\sigma_d(\omega_k)}{median[\sigma_d(\omega)]}\right]^2}{N} \qquad (3)$$

ω is the vector of all frequency components of interest used in the fitting procedure, $\mathcal{E}$ and σ are the measured permittivity and conductivity as given in [22], while $\mathcal{E}_d$ and σ_d are the calculated permittivity and conductivity from either the Cole-Cole [13] or the Debye Formulation derived in this work.

B. Genetic Algorithm

Using Matlab optimization toolbox based on the genetic algorithm GA, the permittivity and conductivity values over the band of interest are fitted to a fourth-order Debye model. The toolbox software tries to find the minimum of the objective function € in (3).

The genetic algorithm (GA) is an evolutionary heuristic algorithm that provides useful solutions to search problems and both constrained and unconstrained optimization problems [23]-[25]. In GA, a population of strings encodes a candidate solution called individual.

A set of Debye parameters $[\mathcal{E}_\infty, \mathcal{E}_1, \mathcal{E}_2, \mathcal{E}_3, \mathcal{E}_4, \tau_1, \tau_2, \tau_3, \tau_4, \sigma_s]$ is an individual to which the objective function is applied. The value of the objective function for an individual is its score. The optimization usually starts from a population of M randomly generated individuals and happens in generations. The population is represented by an M-by-10 matrix. In each generation or iteration, the score of every individual in the population is evaluated; multiple individuals are stochastically selected from the current population based on their score value and used as parents to produce children for the next generation (iteration). To form a new population, the children are produced either by making random changes to a single parent-mutation or by combining the vector entries of a pair of parents-crossover. Over successive generations, the population evolves toward an optimal solution of less objective function.

Commonly, the algorithm terminates when either a maximum number of generations is produced, or a satisfactory fitness level is reached for the population [23]. In this work, the algorithm is terminated when satisfactory solution with minimum objective function is achieved.

C. Optimization Output

Table I presents the Debye parameters of 17 individual head tissues. However, the parameters of the model are intercorrelated to the extent that there is no unique solution. Fig. 1 depicts the electrical properties of the main head tissues based on the measure data [22], derived fourth-order Debye and Cole-Cole model.

The Debye formulation demonstrates an excellent agreement with the measured properties of the head tissues over the frequency band 0.1-3 GHz. Moreover, the derived Debye model is more accurate than the Cole-Cole model at the microwave frequencies of interest. It is essentially indistinguishable from the experiment data. The Cole-Cole model diverges from the measured data and show an obvious disagreement in the permittivity and conductivities in almost each tissue.

Table II shows the error measure as defined in (3) for the new developed Debye model compared with the error estimated using the Cole-Cole model in [13], over the frequency band of interest. Reviewing all the investigated head tissues, we can claim that the developed Debye model results in a very low error measure. Hereby, incorporating the derived fourth-order Debye model in an FDTD simulation would achieve low computational process and high accurate results compared to that based Cole-Cole model or the second-order Debye model.

TABLE I. QUADRATURE-POLE DEBYE MODEL'S PARAMETERS OF HEAD TISSUES

Tissue Type	ε_∞	$\Delta\varepsilon_1$	$\Delta\varepsilon_2$	$\Delta\varepsilon_3$	$\Delta\varepsilon_4$ *10^3	τ_1 ps	τ_2 ps	τ_3 ns	τ_4 µs	σ_s mS/m
Skin Dry	6.6	23.662	9.454	29.787	41.33	4.122	35.7	1.332	1.075	24.2
Skin Wet	2.26	33.493	11.539	14.2	61.365	4.618	36.7	0.553	1.301	109.2
Fat	2.165	2.355	1.513	16.806	1.258	7.386	667	8.783	2.8814	7.6
Bone (cortical)	1	10.367	2	5.75	1.099	10	126.64	1.304	6.12	52.7
Bone (cancellous)	1.428	16.045	3.918	25.65	501.4	9.154	245.1	2.152	7.04	9.3
White Matter	1	33.009	5.902	45.645	1.028	8.261	127.4	1.795	21.134	268.6
Grey Matter	1.373	16.642	31.444	59.869	11.8	0.1	21.51	1.304	1.127	365.5
Blood	2.53	42.125	11.338	703.167	5.013	4.228	36.24	9.639	1.003	999.8
CSF	1.136	48.55	18.692	3055	35.094	2.5	20.01	0.276	1	999.7
Dura	2.164	42.472	4.914	16.53	2.129	9.468	122.1	0.971	74.31	599.8
Bone marrow	1.613	3.096	1	10.546	0.29	6.67	189.7	6.73	22.093	9.8
Cerebellum	1.556	45.914	4.782	328.93	244.1	8.548	213.6	4.538	48.125	146.7
Spinal Chord	4.27	27.5	4.129	112.428	0.386	9.587	237.35	3.49	13.172	166.4
Eye Tissue	3.911	48.303	6.741	1146	69.03	0.1	208.9	16.35	2.27	2.5
Cartilage	1	36.115	7.32	426.486	28.1	0.1	184.9	7.258	59.22	22.3
Muscle Parallel	1.861	51.2	9.646	33.748	84. 6	7.92	97.6	1.477	1.256	113.8
Muscle Transverse	2.807	51.175	9.44	33.457	86.263	8.78	141.3	1.524	1.26	62.5

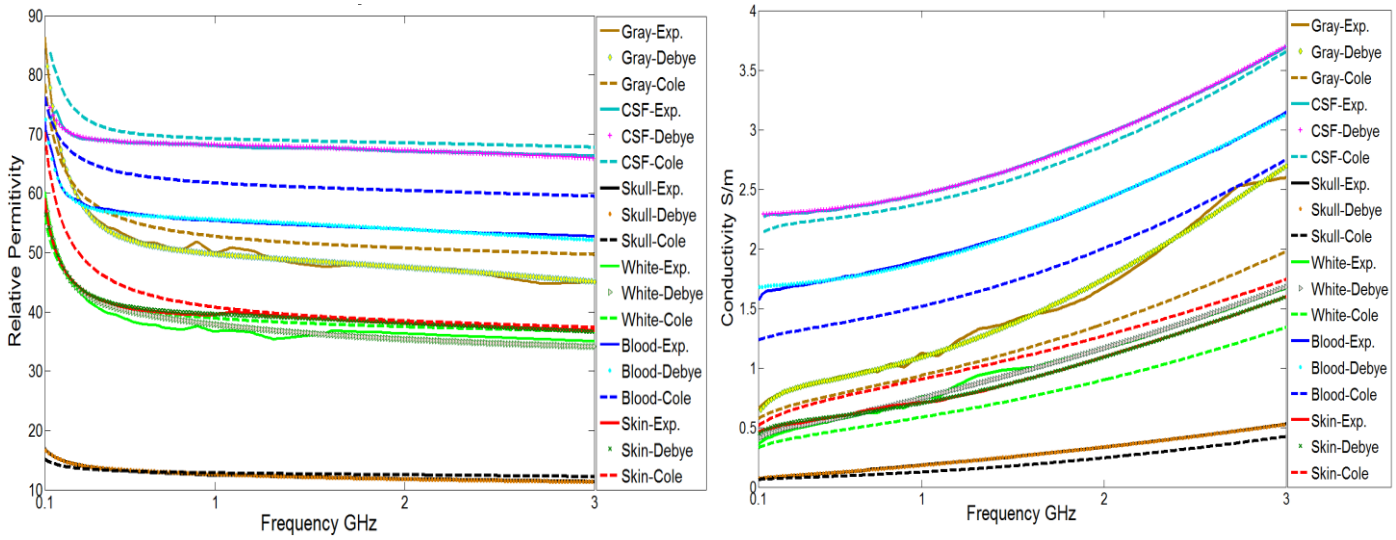

(a) Permittivity (b) Conductivity

Fig. 1 Properties of head tissues with frequency using the derived fourth-order Debye model, and Cole-Cole model compared with the measured data.

TABLE II. VALUES OF ERROR FUNCTION WHEN USING THE DERIVED DEBYE COMPARED WITH COLE-COLE MODEL

Tissue Type	4th order Debye	Cole-Cole
Skin Dry	8.9E-5	0.029
Skin Wet	2.7E-5	0.0455
Fat	1.29E-3	0.0358
Bone (Cortical)	1.1E-4	0.1722
Bone (Cancellous)	1.49E-4	0.025
White Matter	1.3E-3	0.0999
Grey Matter	1.08E-3	0.1059
Blood	7.5E-5	0.0628
CSF	1.9E-5	1.9E-3
Dura	5.2E-05	0.0765
Bone marrow	3.2E-3	0.3788
Cerebellum	6.9E-5	0.0102
Spinal Chord	8.7E-5	0.0220
Eye Tissue	5.9E-5	0.0274
Cartilage	1.1E-4	0.0188
Muscle Parallel	1.2E-4	0.2033
Muscle Transverse	7.7E-5	N/A

III. FORMULATION OF 3D-FDTD FOR THE HEAD

The field distribution in the head tissues can be obtained from the solution of Maxwell's equations using numerical techniques like FDTD. Based on the FDTD method, the time-dependent Maxwell's equations in partial differential form are discretized using central-difference approximations to the space and time partial derivatives. In this work, an FDTD formulation that is based on the convolution approach is used. The relaxation-based dispersive properties of human head tissues are modeled by the derived fourth-order Debye model.

The frequency domain relationship between any component of the electric flux density D(ω) and its related component of the electric field E(ω) is given by

$$D(\omega) = \mathcal{E}_0 \mathcal{E}_r^{'}(\omega)\, E(\omega) \tag{4}$$

where

$$\mathcal{E}_r^{'}(\omega) = \mathcal{E}(\omega) + j\,\sigma(\omega) \tag{5}$$

$\mathcal{E}_o$ is the vacuum permittivity. The complex relative permittivity $\mathcal{E}_r^{'}(\omega)$ as a function of angular frequency is given by (2). The inverse Fourier transform ($\mathfrak{F}^{-1}$) of the multi-pole term $\left(\sum_{i=1}^{P} \frac{\Delta\mathcal{E}_i}{1+j\omega\tau_i}\right)$ is

$$\mathfrak{F}^{-1}\left[\sum_{i=1}^{P} \frac{\Delta\mathcal{E}_i}{1+j\omega\tau_i}\right] = \begin{cases} \sum_{i=1}^{P} \frac{\Delta\mathcal{E}_i}{\tau_i} \int_0^t e^{-t/\tau_i}\, dt & for\ t \geq 0 \\ 0 & for\ t < 0 \end{cases} \tag{6}$$

It is also known that the inverse Fourier transform ($\mathfrak{F}^{-1}$) of the term $\frac{1}{j\omega}$ is the unit step function u(t). Thus, the electric flux density in the time domain can be determined by the convolution as

$$D(t) = \mathcal{E}_0\, \mathcal{E}_\infty E(t) + \sum_{i=1}^{P} \frac{\Delta\mathcal{E}_i.\mathcal{E}_0}{\tau_i} \int_0^t e^{-(\mathfrak{t}-t)/\tau_i}.\ E(\mathfrak{t})d\mathfrak{t} + \sigma_s \int_0^t E(\mathfrak{t})d\mathfrak{t} \tag{7}$$

and in the sampled time domain

$$D^n = \mathcal{E}_0\, \mathcal{E}_\infty E^n + \sum_{i=1}^{P} \frac{\Delta\mathcal{E}_i.\mathcal{E}_0.\Delta t}{\tau_i} \sum_{h=0}^{n} e^{-\Delta t(n-h)/\tau_i}.E^h + \sigma_s.\Delta t \sum_{h=0}^{n} E^h \tag{8}$$

The time is specified by the superscript n, i.e. $t = n.\Delta t$. By separating the electric field, i.e. the term E^n, from the rest of the summation, we get

$$E^n = \frac{D^n - \mathcal{E}_0\,.\xi^n}{(\mathcal{E}_0\, \mathcal{E}_\infty + \sum_{i=1}^{P} \frac{\Delta\mathcal{E}_i\,.\mathcal{E}_0.\Delta t}{\tau_i} + \sigma_s.\Delta t)} \tag{9}$$

where

$$\xi^n = \sum_{i=1}^{P} \frac{\Delta\mathcal{E}_i.\mathcal{E}_0.\Delta t}{\tau_i} \sum_{h=0}^{n-1} e^{-\Delta t(n-h)/\tau_i}.E^h + \sigma_s.\Delta t \sum_{h=0}^{n-1} E^h \tag{10}$$

The electric field components Ez, Ey and Ex are found using (9) which is applicable to any of those components. The corresponding electric flux density update equation based on Ampere's law and the magnetic field components update equation based on Faraday's law are given in Appendix A.

IV. SIMULATION RESULTS

To test the derived Debye model and 3D-FDTD formulation, anatomically realistic FDTD head model is used. That model is derived using high-resolution magnetic resonance imaging (MRI) head scans [26]. The model includes 128 transverse slices and consists of 256×256×128 cubical elements, with a data-set to indicate what tissue each element belongs to. The three dimensional head used in the simulations is illustrated in Fig. 2.

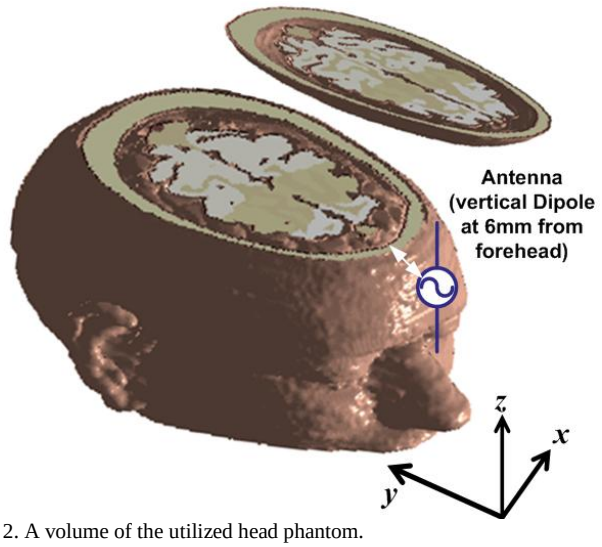

Figure 2. A volume of the utilized head phantom.

The FDTD calculation is carried out with the time step of 2.12 psec and a spatial grid of cubic Yee cells with discretization of Δx = Δy = Δz =1.1 mm. The computational domain is surrounded by an absorbing layer as an aggregate of Perfectly Matched Layer (PML) media to keep outgoing electric and magnetic fields from being reflected back into the computational domain. The simulation head medium is irradiated by a microwave Gaussian pulse covering the band from DC to around 6 GHz. A z-polarized incident wave is illuminated by a half-wavelength dipole antenna at 6 mm from the forehead at a position indicated in Fig. 2. The simulation is

iterated at different time steps till the time when the radiated pulse has died out.

The field inside the phantom is illustrated by $|E_z|$ distribution in Fig. 3 on a transverse slice in *xy* plane at approximately 42 mm from the crown of the head. Moreover, electric field intensity distribution |Ey| on a transverse slice in xz plane at approximately 41 mm from the forehead of the face is depicted in Fig. 4. The color bars show the degradation in the field strength with higher number of iterations, i.e. longer time since applying the source.

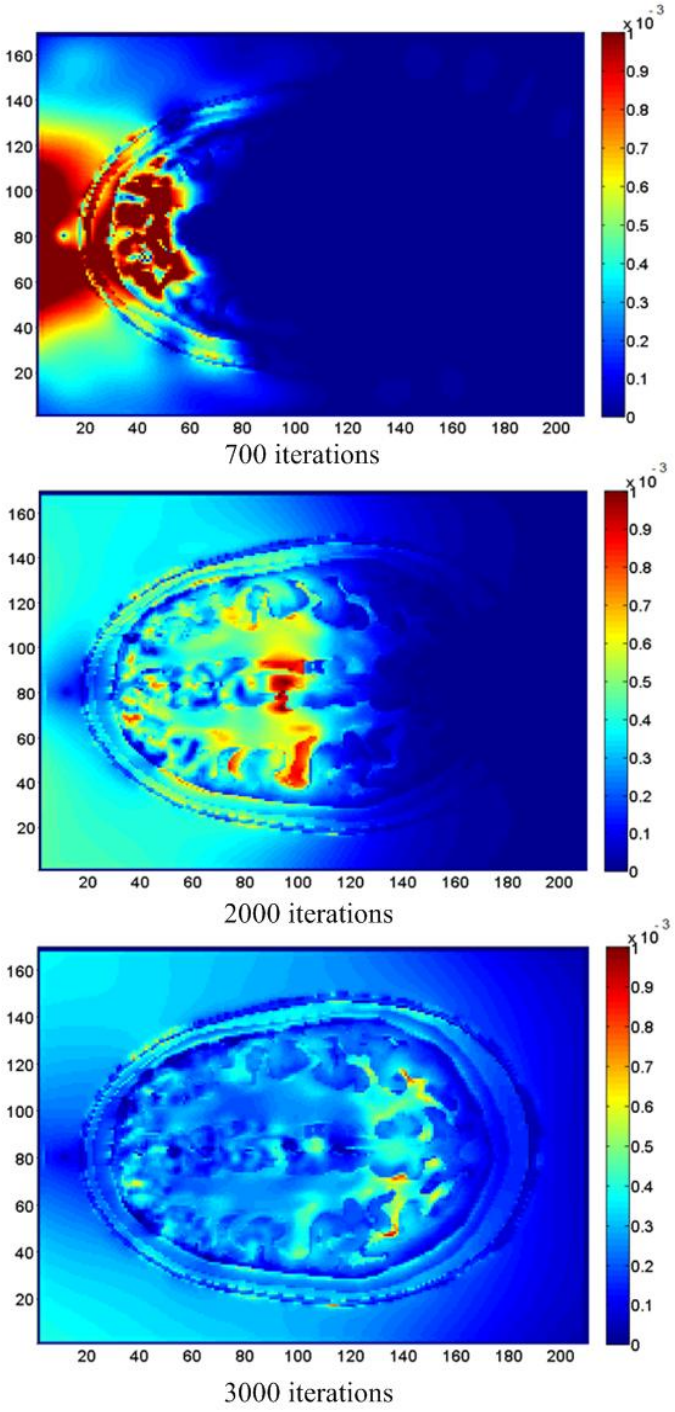

Figure 3. Transverse view of |Ez| distribution in the head.

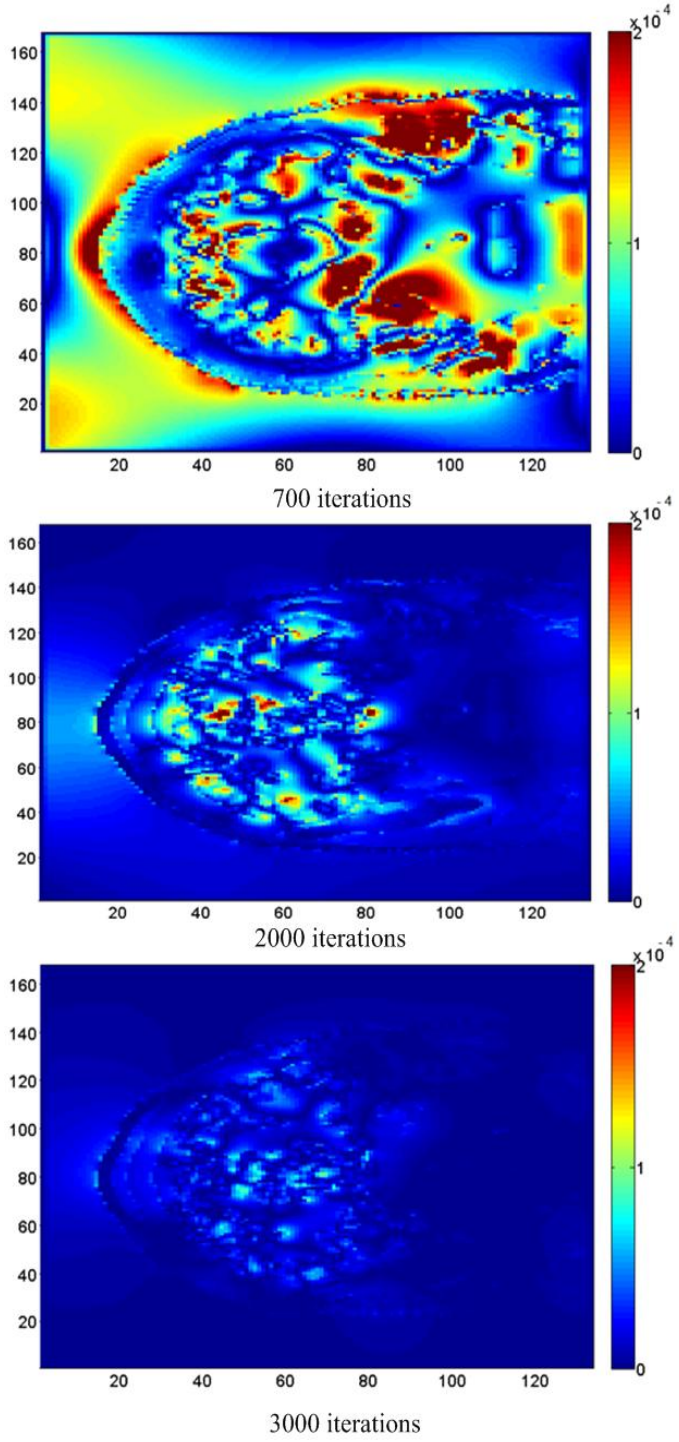

Figure 4. Transverse view of |Ey| distribution in the head.

From the presented result in Fig. 3, it can be clearly seen that the field penetrates the head tissues progressively with time (number of FDTD iterations). As expected, the field is significantly attenuated while penetrating the head. However, the field reaches the other side of the head since the utilized pulse includes low microwave frequencies. The decay in the field is also demonstrated in Fig. 4 which shows |Ey| at three time steps of the same head slice. It is worth mentioning that since the field shown in Fig. 4 is cross-polarized, it has

significantly lower values (less by around 20 dB) compared with the co-polarized fields depicted in Fig. 3.

Since the head is roughly anatomically symmetrical with respect to the central line that divides the head into left and right halves, and the dipole antenna faces that central lines, the distribution of the field inside the head is roughly symmetrical with respect to the central line as depicted in Figs. 3 and 4.

The time needed for the simulation using our developed convolution-based FDTD formulation is compared with the differential-based FDTD formulation [21] and MOM. Since the formulation in [21] is two-dimensional, we consider a two-dimensional simulation by extracting a transverse slice of the three-dimensional phantom for a fair comparison. Using Matlab 7 64-bit, on an Intel® Core™ 2 Due CPU with 4 GB of RAM, the FDTD solver in this work takes 298 seconds to compute 10,000 time steps. The FDTD solver based on the differential approach [21] takes 446 seconds, whereas the MOM solver takes 856 seconds to compute 10,000 time steps. All the solvers segment the same transverse slice of the head phantom with 1.1mm x 1.1mm cells. Despite using the highly accurate fourth-order Debye model, the convolution-based FDTD solver of this work needs only two-thirds of the time required by the differential-based FDTD solver.

To show the field distribution at different frequencies, discrete Fourier transform is applied at each time step during the 3000 FDTD iterations to the cells indexed by i, j, k, as given by

$$E_z^f(i,j,k) = \sum_{n=1}^{Nt} E_z^n(i,j,k).\ \exp(-j2\pi n.\Delta t.f) \qquad (11)$$

Fig. 5 portrays the field distribution at 0.1 GHz. It is obvious that the field starts to penetrate the head tissues. At the iteration (3000), the wave reaches around the center of the head. Since the head is roughly anatomically symmetrical with respect to its central line, the distribution of the field inside the head is roughly symmetrical with respect to that line.

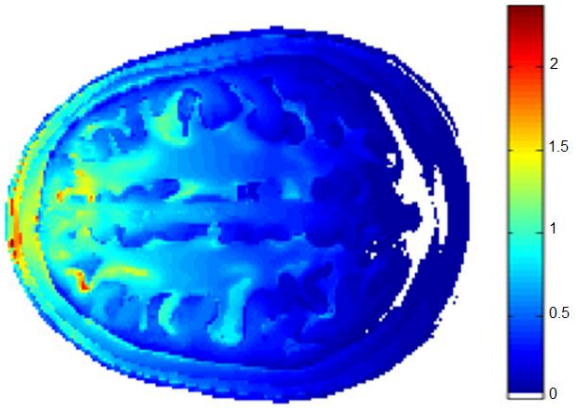

Figure 5. Transverse view of $|E_z^f|$ at 0.1 GHz after 3000 FDTD iterations.

Fig. 6 investigates the field distribution and penetration depth into the head at different frequencies of interest where different depths are recorded. It is clear from the presented results that the signal at 0.5 GHz easily penetrates the head tissues. The penetration depth decreases quite significantly when using the frequency 2 GHz. Thus, it is expected that the band from around 0.5 GHz to 1.5 GHz could be the best option for microwave imaging of the head.

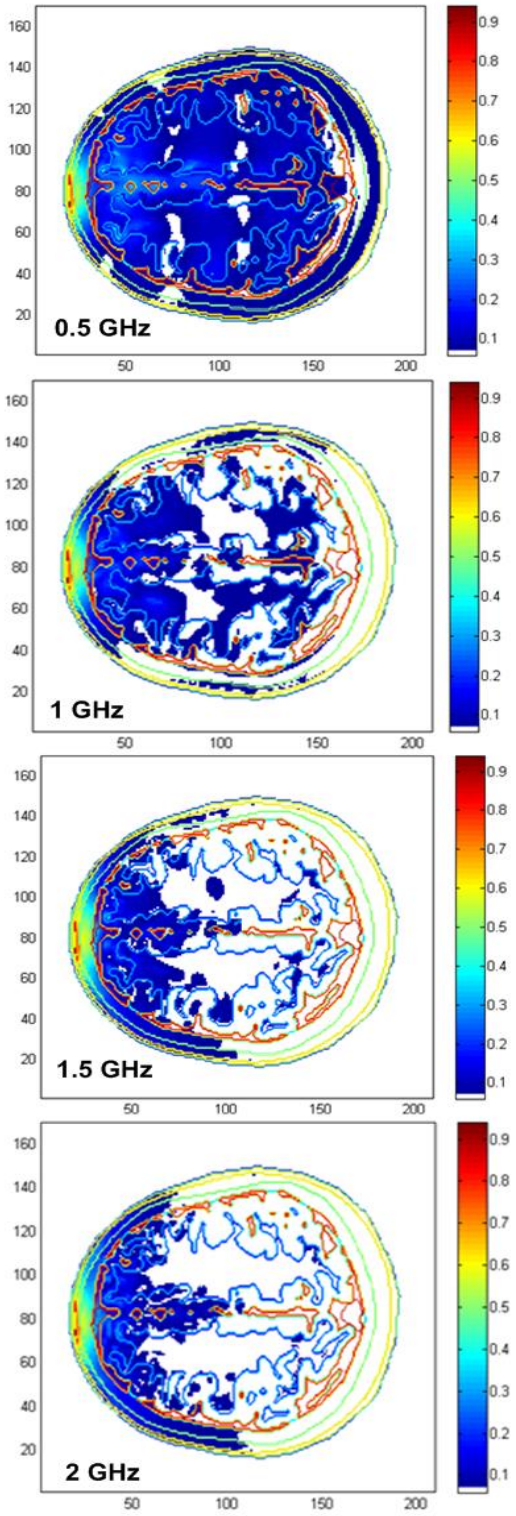

Figure 6. Transverse view of $|E_z^f|$ distribution at 0.5, 1, 1.5 and 2 GHz.

To verify the proposed Debye models and the FDTD methodology, the computed fields inside the head phantom are compared to those obtained using the commercial software (CST Microwave Studio) which is based on the finite integration technique.

Since CST does not include a realistic numerical head phantom with the accurate realistic properties, we created that numerical head phantom from the slices used in our FDTD simulations. The process of creating CST head model includes processing high-resolution magnetic resonance images of a head that consists of 256×256×128 cubical elements from [1] followed by creating voxel data and preparing tissue property files. The voxel data was then written into voxel data file which has resolution of 1.1 mm× 1.1 mm× 1.1 mm. The measured electrical properties of the head tissues [22] were used as property sources in the simulation tool. These properties are saved separately according to voxel types. The property files are then assigned to specific voxels defined by voxel data file in CST. The final head phantom has the same distribution of tissues compared to the model used in our FDTD calculations (Fig. 2). In the CST and FDTD solvers, a wide band Gaussian wave polarized perpendicular to the xy plane of the phantom was used as an excitation source.

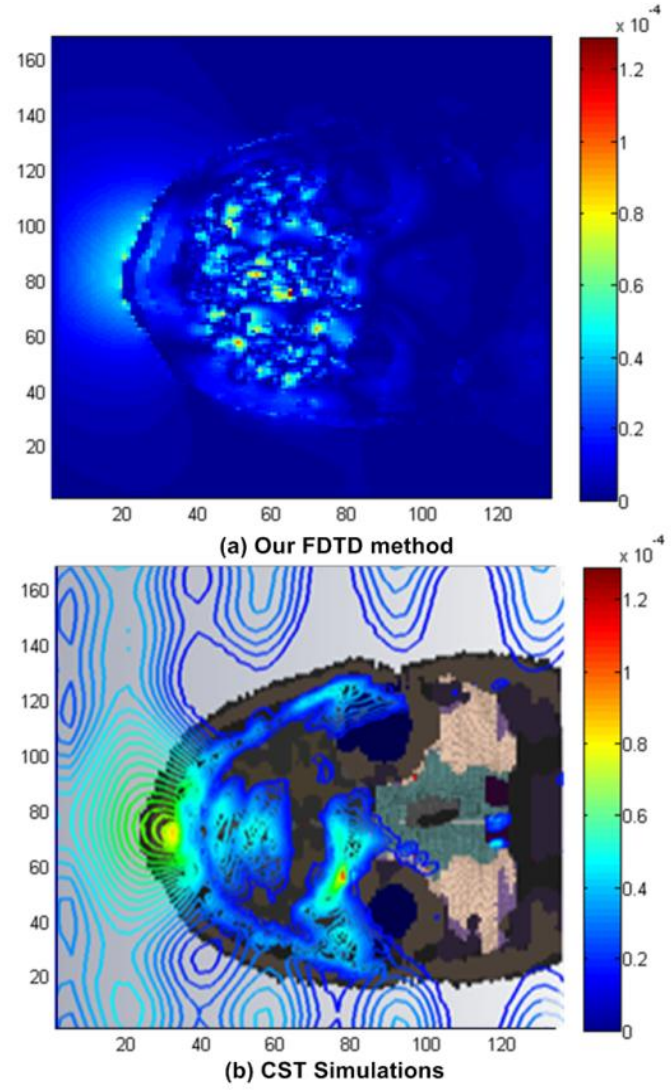

Figure 7. Comparison between the calculated |Ey| distributions after 3000 iterations using the proposed method with 4th order Debye model and the simulated distribution using CST Microwave Studio with the measured properties at the same time step.

The computed fields inside the three dimensional head phantom are compared to CST field distribution. As an example, the calculated |Ey| fields in a slice at approximately 30 mm from the forehead after 3000 iterations using the proposed FDTD methodology and CST Microwave Studio are depicted in Fig. 7. The properties of the head tissues in the simulations were the same measured values from [22], whereas the derived 4th order Debye model was used in our method.

The two calculated fields shown in Fig. 7 have a reasonable agreement in the range of values as clarified by the same scale range in the associated color bars, and the same general distribution along the selected slice. The discrepancies between the two fields in Fig. 7 come from two factors. The first one is the difference in dispersive models for the dielectric properties of the head tissues. While our model guarantees a perfect agreement with the measured data, the CST solver uses a simple fitting that does not agree well with all the measured data across the utilized band. The second factor comes from the fact that CST solver uses a real model for the dipole antenna with its narrowband performance, whereas a simple model of the dipole antenna as a hard source is included in the Matlab code used in our FDTD methodology.

V. Conclusion

Using a genetic algorithm, the fourth-order Debye models for the complex permittivity of 17 different head tissues have been derived. The model gives an accurate estimation of the dispersive properties of the human head tissues across the frequency band from 0.1 GHz to 3 GHz which can be used for microwave imaging of the head. The developed Debye model is used in a three-dimensional finite-difference time-domain formulation to accurately predict the interaction of electromagnetic fields with the human head tissues.

Appendix A

In this work, the electric filed components E_z, E_x and E_y are found at each time step (n) using (9), and the corresponding electric flux density update equation are derived using Ampere's law as given by

$$D_z^{n+1}(i,j,k) = D_z^n(i,j,k) + \frac{\Delta t}{\Delta x}[H_y^{n+\frac{1}{2}}(i,j,k) - H_y^{n+\frac{1}{2}}(i-1,j,k)] - \frac{\Delta t}{\Delta y}[H_x^{n+\frac{1}{2}}(i,j,k) - H_x^{n+\frac{1}{2}}(i,j-1,k)] \quad \text{(A1)}$$

$$D_y^{n+1}(i,j,k) = D_y^n(i,j,k) + \frac{\Delta t}{\Delta z}[H_x^{n+\frac{1}{2}}(i,j,k) - H_x^{n+\frac{1}{2}}(i,j,k-1)] - \frac{\Delta t}{\Delta x}[H_z^{n+\frac{1}{2}}(i,j,k) - H_z^{n+\frac{1}{2}}(i-1,j,k)] \quad \text{(A2)}$$

$$D_x^{n+1}(i,j,k) = D_x^n(i,j,k) + \frac{\Delta t}{\Delta y}[H_z^{n+\frac{1}{2}}(i,j,k) - H_z^{n+\frac{1}{2}}(i,j-1,k)] - \frac{\Delta t}{\Delta y}[H_y^{n+\frac{1}{2}}(i,j,k) - H_y^{n+\frac{1}{2}}(i,j,k-1)] \quad \text{(A3}$$

where (i,j,k) are the cell spatial indices. The finite –difference update equations for the magnetic field components are derived from Faraday's law as given by

$$H_z^{n+\frac{1}{2}}(i,j,k) = H_z^{n-\frac{1}{2}}(i,j,k) + \frac{\Delta t}{\mu_o * \Delta y}[E_x^n(i,j+1,k) - E_x^n(i,j,k)] - \frac{\Delta t}{\mu_o * \Delta x}[E_y^n(i+1,j,k) - E_y^n(i,j,k)] \quad \text{(A4)}$$

$$H_y^{n+\frac{1}{2}}(i,j,k) = H_y^{n-\frac{1}{2}}(i,j,k) + \frac{\Delta t}{\mu_o * \Delta x}[E_z^n(i+1,j,k) - E_z^n(i,j,k)] - \frac{\Delta t}{\mu_o * \Delta z}[E_x^n(i,j,k+1) - E_x^n(i,j,k)] \quad \text{(A5)}$$

$$H_x^{n+\frac{1}{2}}(i,j,k) = H_x^{n-\frac{1}{2}}(i,j,k) + \frac{\Delta t}{\mu_o * \Delta z}[E_y^n(i,j,k+1) - E_y^n(i,j,k)] - \frac{\Delta t}{\mu_o * \Delta y}[E_z^n(i,j+1,k) - E_z^n(i,j,k)] \quad \text{(A6)}$$

μ_o is the vacuum permeability.

ACKNOWLEDGMENT

The authors acknowledge the useful discussions with Dr. David Ireland from School of ITEE, The University of Queensland.

REFERENCES

[1] R. Amineh, A. Khalatpour, N. Nikolova, "Three-dimensional microwave holographic imaging using co- and cross-polarized data," *IEEE Trans Antennas Prop*, vol.60, no.7, pp.3526-3531, 2012.

[2] A Abbosh, S Crozier, "Strain imaging of the breast by compression microwave imaging," *IEEE Ant Wireless Prop Lett*, vol. 9, pp. 1229-1232, 2010.

[3] A. Abubakar, T. Habashy, P. Guangdong M. Li, "Application of the multiplicative regularized Gauss–Newton algorithm for three-dimensional microwave imaging," *IEEE Trans Antennas Prop*, vol.60, no.5, pp.2431-2441, 2012.

[4] B. Mohammed, D. Ireland, A. Abbosh, "Experimental investigations into detection of breast tumor using microwave system with planar array," *IET Microwaves Antennas Prop*, vol. 6, no. 12, pp. 1311-1317, 2012.

[5] D. Ireland, K. Bialkowski, A. Abbosh, "Microwave imaging for brain stroke detection using born iterative method," *IET Microw. Antennas Propag*, vol.7, no.11, pp. 909-915, 2013.

[6] X. Zeng, A. Fhager, M. Persson, P. Linner, H. Zirath, "Accuracy evaluation of ultrawideband time domain systems for microwave imaging," *IEEE Trans Antennas Prop*, vol.59, no.11, pp.4279-4285, 2011.

[7] S. Mustafa, B. Mohammed, A. Abbosh, "Novel preprocessing techniques for accurate microwave imaging of human brain," *IEEE Ant Wireless Prop Lett*, vol. 12, pp .460-463, 2013.

[8] B. Mohammed, A. Abbosh, D. Ireland, "Stroke detection based on variations in reflection coefficients of wideband antennas," *IEEE Int. Symp. Antennas and Propagation*, Chicago, USA, 2012.

[9] B. Mohammed, A. Abbosh, S. Mustafa, D. Ireland, D., "Microwave system for head imaging," *IEEE Trans Instrumentation and Measurement*, vol.63, no.1, pp.117-123, 2014.

[10] Y. Serguei, Y. Semenov and D.R. Corfield, "Microwave tomography for brain imaging: feasibility assessment for stroke detection," *Int. J. Antennas Prop.*, vol. 2008, Article ID 254830, 2008.

[11] D. Ireland, M.E. Bialkowski, "Feasibility study on microwave stroke detection using a realistic phantom and the FDTD method," *Asia-Pacific Microwave Conference*, pp.1360-1363, 2010

[12] N. Simicevic and D. T. Haynie, "FDTD simulation of exposure of biological material to electromagnetic nanopulses," *Phys. Med. Biol.*, vol.50, pp. 347-360, 2005.

[13] S. Gabriel, R. W. Lau and C. Gabriel, "The dielectric properties of biological tissues: III. Parametric models for the dielectric spectrum of tissues, *Physics Medicine and Biology*, vol. 41, no.11, 1996.

[14] F. L. Teixeira, "Time-domain finite-difference and finite-element methods for Maxwell equations in complex media," *IEEE Trans. Antennas Propagation*, vol. 56, no. 8, pp. 2150-2166, 2008.

[15] M. R. Tofighi, "FDTD modeling of biological tissues Cole-Cole dispersion for 0.5-30 GHz using relaxation time distribution samples-Novel and improved implementations," *IEEE Trans. Microw. Theory Tech.*, vol. 57, no. 10, pp. 2588-2596, 2009.

[16] B. Guo, J. Li, and H. Zmuda, "A new FDTD formulation for wave propagation in biological media with Cole-Cole model," *IEEE Microw. Wireless Compon. Lett.*, vol. 16, no. 12, pp. 633-635, 2006.

[17] F. Torres, P. Vaudon, and B. Jecko, "Application of fractional derivatives to the FDTD modeling of pulse propagation in a Cole–Cole dispersive medium," *Microwave Opt Tech. Lett*, vol. 13, no. 5, pp. 300-304, 1996.

[18] I. T. Rekanos, and T.G. Papadopoulos, "FDTD Modeling of Wave Propagation in Cole-Cole Media With Multiple Relaxation Times," *IEEE Antennas Wireless Prop. Lett.*, vol. 9, pp. 67- 69, 2010.

[19] J. M. Schuster and R. J. Luebbers, "An FDTD algorithm for transient propagation in biological tissue with a Cole–Cole dispersion relation," in *Int. Symp. Antennas Propag.* vol. 4, pp. 1988–1991, 1998.

[20] M. Lazebnik, M. Okoniewski, J. H. Booske, and S. C. Hagness, "Highly accurate Debye models for normal and malignant breast tissue dielectric properties at microwave frequencies," *IEEE Microw. Wireless Compon. Lett.*, vol. 17, no. 12, pp. 822–824, 2007.

[21] D. Ireland, and A. Abbosh, "Modeling human head at microwave frequencies using optimised Debye models and FDTD method," *IEEE Trans Antennas Prop*, vol.61, no.4, pp.2352-2355, 2013.

[22] "Dielectric Properties of Body Tissues in the Frequency Range 10Hz - 100GHz," [Online], Available: http://niremf.ifac.cnr.it/tissprop/.

[23] D. Goldberg, B. Korb, and K. Deb, "Messy genetic algorithms: Motivation, analysis, and first results," The Clearinghouse for Genetic Algorithms (TCGA), Report 89003, 1989.

[24] M. Gen, R. Cheng, Genetic Algorithms and Engineering Optimization, Wiley, 2000.

[25] J. Zhang, H. Chung and W. L. Lo, "Clustering-based adaptive crossover and mutation probabilities for genetic algorithms," *IEEE Trans Evolutionary Comp*, vol.11, no.3, pp.326-335, 2007.

[26] I.G. Zubal, C.R. Harrell, E.O. Smith, Z. Rattner, G. Gindi and P.B. Hoffer, "Computerized three-dimensional segmented human anatomy," *Medical Physics*, vol. 21, no. 2, pp.299-302, 1994.